Quantum Chemical Studies on Metal Organic Frameworks: Catalysis and Separation

by

Sen Zhang

B.S. in Applied Chemistry, Shandong University, 2017

Submitted to the Graduate Faculty of

Swanson School of Engineering in partial fulfillment

of the requirements for the degree of

Master of Science in Chemical Engineering

University of Pittsburgh

2019

UNIVERSITY OF PITTSBURGH

SWANSON SCHOOL OF ENGINEERING

This thesis was presented

by

Sen Zhang

It was defended on

March 27, 2019

and approved by

J Karl Johnson, Ph.D., W. K. Whiteford Professor
Department of Chemical and Petroleum Engineering

Götz Veser, Ph.D., Professor
Department of Chemical and Petroleum Engineering

Nathaniel L Rosi, Ph.D., Professor
Department of Chemistry

Thesis Advisor: J Karl Johnson, Ph.D., W. K. Whiteford Professor
Department of Chemical and Petroleum Engineering

Quantum Chemical Studies on Metal Organic Frameworks: Catalysis and Separation

Sen Zhang, M.S.

University of Pittsburgh, 2019

Metal-organic frameworks, one emerging class of solid nanoporous materials, have unique chemistries in gas storage, gas separation, catalysis, and many other fields. The goal of this work is to develop new MOFs for reactions and separations. Two metal-organic frameworks (MOFs) were investigated to 1) synthesize formaldehyde from syngas as a heterolytic catalyst, 2) separate the paraffin from the olefin-paraffin mixture.

Table of Contents

List of Tables

List of Figures

Preface

I would like to express my gratitude to my supervisor Dr. J Karl Johnson for his kind help, useful comments, and engagement through the learning process of my master thesis. Moreover, I would like to thank Lin Li for introducing me to these projects as well for the support and collaboration on the way. Also, I would like to thank other collaborators. Furthermore, I would like to acknowledge my committee member, Dr. Veser, and Dr. Rosi for their insightful comments and feedbacks. Last but not least, I would like to thank my friends and family for providing me with encouragement throughout my years of study.

1.0 **Introduction**

Metal-organic frameworks (MOFs) is one emerging class of solid nanoporous materials. As its name indicates, MOFs are composed of both inorganic building units and organic linkers. Figure 1 shows the simplified process for MOF synthesis, the dark gray cubes represent the inorganic building units, the gray cuboids represent the organic linkers. A large number of available metal centers and organic linkers can be combined together via various coordination modes, tremendous multidimensional types of MOFs can hence be synthesized. MOFs have been studied for their potential use in many fields, including gas storage, gas separation, catalysis, luminescent sensor,[1] and drug delivery.[2]

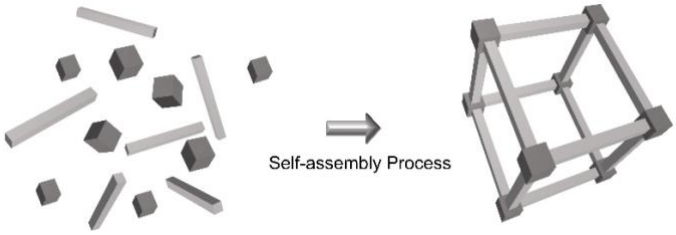

Figure 1. MOF self-assembly process.

Besides the experimental investigation approach, the high crystallinity of MOFs makes it a material also suitable for computational studies, which offers the possibility to investigate the properties that cannot be easily detected by experiments to give valuable insights and to predict performance.

1.1 **Direct formaldehyde synthesis from syngas**

Due to the large demands and the great importance of formaldehyde in industry as a chemical platform,[3] synthesizing formaldehyde in an energy-efficient and low-cost way is a popular research area. The Fischer-Tropsch reactions developed in the early 1920s plays the key role in the current industrial method to synthesize formaldehyde from carbon monoxide and hydrogen.[4-5] This hydrogenation reaction is typically catalyzed by using transition metals. The reaction mechanisms for this process have been well explained.[6-7] However, such a multi-step process requires high operation temperatures and faces the difficulty in product separation.[8-9] New catalysts are in demands for reducing the cost and improving the energy utilization efficiency of formaldehyde synthesis.[10-12]

Since the Frustrated Lewis Pairs (FLPs) concept was proposed by Stephan et al. a decade ago, the activation of small inert molecules and bonds was no longer particularly limited to the transition metals or transition metal containing compounds.[13-14] The unquenched Lewis base site and acidic site, which are prevented from self-quenching by steric hindrance, give rise to the unique chemical properties of the FLPs. Work done by many research groups have shown the high reactivity of FLPs for the heterolytic cleavage of dihydrogen, and this hydrogen split reactivity of FLPs triggers a large number of new approaches for many chemical reactions, especially for the hydrogenation reaction.[15-18] Previously, our group computationally designed a new catalyst, UiO-67-NBF_2, that incorporates a catalytic active geminal aminoborane-based FLP moiety into a robust Metal-organic Framework UiO-67.[19-20] This new catalyst could potentially lead to a dramatic reduction of the cost of CO_2 capture and conversion to methanol. These results suggest the possibility of directly converting syngas (a mixture of CO and H_2) to formaldehyde by using UiO-67-NBF_2 as a heterolytic catalyst.

In chapter 3, we investigated the feasibility of synthesizing formaldehyde via the mediation of a geminal aminoborane-based FLP moiety in UiO-67-NBF_2. My research focused on the investigation on the FLP moiety. The uncatalyzed gaseous reaction thermodynamics were calculated at the complete basis set. The reaction pathway for both uncatalyzed and the FLP moiety catalyzed gaseous reaction were investigated by using DFT methods and high-level *ab initio* methods. The direct hydrogenation of CO to formaldehyde was shown to be kinetically feasible with this LPs moiety. My results were combined with work from L. Li and J.P. Ruffley on periodic models, resulting in a paper published in *ACS Sustainable Chemistry & Engineering*.[21]

1.2 **Olefin-paraffin Separation**

MOFs are also widely investigated in the gas separation field due to its large surface area, tunable pore structure and chemistry. Among the many separation methods, separation by adsorption is recognized as a promising approach and can be realized through different mechanisms such as thermodynamic equilibrium, molecular sieving, and kinetic mechanisms.[22]

In chapter 4, we focus on applying Cu(I)-MFU-4*l*[23] to the separation of olefin and paraffin species via the thermodynamic equilibrium mechanism. This separation is important because hydrocarbons such as olefins (C_2H_4, C_3H_6 etc.) are essential raw chemical feedstocks that can be further converted to daily utilized consumer products or industrial products. However, due to the similar properties of olefins and paraffins, like molecular size and boiling points, olefin-paraffin separation is highly energy intensive and is typically carried out by cryogenic distillation.[24] This process requires many distillation stages, high reflux ratio, and has to be achieved at cryogenic temperature and very high pressure.[22]

The thermodynamic equilibrium adsorption mechanism is based on the affinity differences between the adsorbates and the adsorbent surface. Large pore size and strong attraction are usually required to allow adsorbates to pass and separate the adsorbate mixtures. The binding strength of adsorbates on adsorbent is highly the result of open metal sites within the MOFs, and it can be adjusted by changing the open metal sites. Hence, the thermodynamic equilibrium mechanism is regarded as a most effective way for olefin/paraffin separation. A large number of MOFs with open metal sites have been synthesized and show promising separation performance, like MMOF-74 (M = Co, Mn, Mg, Ni, Zn, Fe),[25-27] MIL-100(Fe),[28-29] (Cr)-MIL-101-SO_3Ag,[30] PAF-1-SO_3-Ag,[31] etc.

In chapter 4, the periodic framework was truncated to a non-periodic 30-atom cluster, the binding energies of a series of molecules were calculated for both the tailored cluster and periodic system using density functional theory (DFT). The cluster model was inspected to see whether it gives accurate descriptions of the binding energies, compared with the full MOF DFT calculations and experimental results. Then we investigated how the Cu(I)-MFU-4*l* makes the olefin/paraffin separation possible. Furthermore, key cluster geometry parameters that control the binding energy were identified and a cluster only allowing Cu atom to move was developed to further lower the computational cost.

2.0 **Methodology**

Kohn-Sham Density functional theory (KS-DFT) is a popular computational modelling method used in physics, chemistry and material science.[32] It describes the many-body systems using electron density functionals, which are the functions of electron density. According to the Hohenberg–Kohn theorems,[33] the ground state of a many-body system is determined uniquely by the electron density which only depends on three-spatial coordinates. This reduces the many-body problem of 3N spatial coordinates to three-spatial coordinates, and we can minimize the energy with respect to the electron density by applying the variational principle. The KS DFT energy functional is in the form of Equation 2-1. The $T_s[\rho]$ term represents the kinetic energy, the $E_{eN}[\rho]$ represents the interaction with external potential, and $J[\rho]$ is the Coulomb interaction. $E_{xc}[\rho]$ is called exchange-correlation functional, which includes all information not included in the first three terms, and it is the only unknown term and must be approximated. Many functionals based on different approximations such as LDA, GGA, etc., have been developed.

$$E_{KS\_DFT}[\rho] = T_s[\rho] + E_{eN}[\rho] + J[\rho] + E_{xc}[\rho] \tag{2-1}$$

Different from DFT, the Hartree-Fock method uses exact, many-electron wavefunction to describe the system, and the many-electron wavefunction takes the form of Slater determinant. Because the general many-electron wavefunction cannot be expressed as a single determinant, the HF method hence neglects the electron correlation, which leads to large deviation from experimental results. Post-Hartree-Fock methods such as Møller–Plesset perturbation (MP) theory[34] and coupled cluster (CC) theory are proposed to offset the weakness.

The MP method adds electron correlation effects by means of Rayleigh–Schrödinger perturbation theory (RS-PT)[35] to improve the Hartree-Fock methods. The CC method constructs multi-electron wavefunctions to account for the electron correlations. The second order Møller–Plesset calculation (MP2) is the standard level used in quantum chemistry, especially for small systems. Higher order methods, such as MP3, MP4, and MP5, are less used because of the cost and because these methods do not always give results better than MP2. The CCSD(T) method (coupled cluster singles, doubles, and perturbative triples) is a higher-level method and is regarded as the gold standard of quantum chemistry for giving the most accurate results without resulting to configuration interaction methods, which are extremely costly from a computational standpoint. These methods, however, are much more sensitive to basis set than the DFT calculations, and mathematically incomplete basis sets will introduce error in calculation results. For such a reason, very large basis sets are required to reproduce the accurate results at the complete basis set (CBS) limit. But it is impractical to employ very large finite basis sets, especially for medium or large systems. One alternative approach is using the extrapolation techniques. In this work, we employ the formula proposed by Helgaker et al.[36] (Equation 3-1) to extrapolate the energies to CBS limit.

The post-Hartree-Fock methods are usually regarded as more accurate than DFT, but they are also more expensive. Things have been changing recently because the DFT techniques are becoming more refined. DFT will be the dominant method used in this work, and only small systems will employ post-Hartree-Fock methods.

The climbing image nudge elastic band (CI-NEB) method[37] is a widely used interpolation algorithm to find the minimum energy pathway (MEP). It generates a sequence of configurations between the initial (reactant) and final (product) configurations. The initial and final configurations are critical to success of the NEB method because if the initial and final states are not actually

connected by a MEP the method will fail. Moreover, the NEB method requires initial guesses for the intermediate images or replicas. If the initial guesses are unphysical or too far from the actual MEP the convergence of the NEB calculation can be extremely slow or the calculation could fail.

The intrinsic reaction coordinate (IRC) calculation was usually performed in order to confirm the saddle point calculated were connected by the two minima. By giving the initial geometry (transition state geometry), the IRC calculation will follow the forward and reverse directions from that point, and produce the minima connected to the TS state. In this work, CI-NEB methods and IRC were used to locate and verify the transition state.

3.0 **Formaldehyde Synthesis from Syngas**

(This work has been published in *ACS Sustainable Chemistry & Engineering*.[21] This chapter reports my contributions to that publication.)

3.1 **Computational Details**

The electronic energy, zero-point energy, enthalpy, and the Gibbs free energy calculations for clusters were all performed in the Gaussian16 program. The D3 correction method, different levels of theory (PBE, B3LYP, MP2, CCSD(T)) and several basis sets (aug-cc-pVXZ (X=T, Q, 5)) were used. All energies were extrapolated to the complete basis set (CBS) using the extrapolation formula (Equation 3-1) proposed by Helgaker et al., where n represents the angular momentum number, a is the fitting parameter. In this work, the energy at the complete basis set limit (E_∞), and a are the intercept and slope, respectively, from linear regression between E_n and $\frac{1}{n^3}$ (n=3, 4, 5).

$$E_n = E_\infty + \frac{a}{n^3} \tag{3-1}$$

The NBF_2 moiety and the Lewis pairs functionalized UiO-67-NBF_2 used for calculations are as shown in Figure 2.

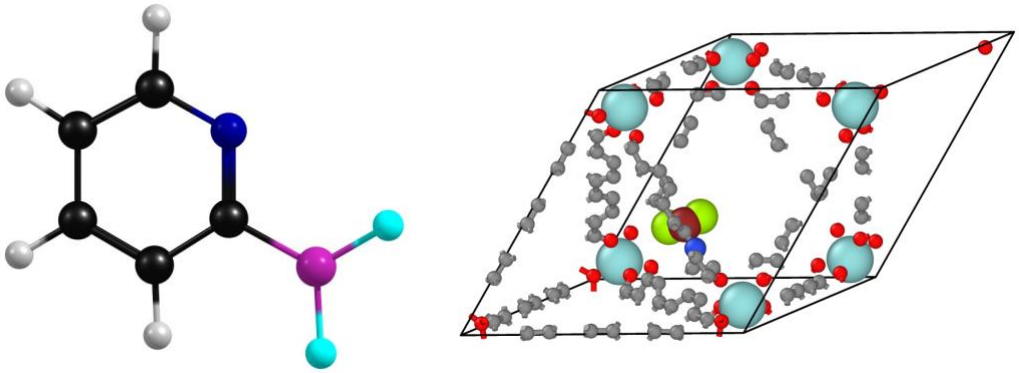

Figure 2. NBF_2 moiety (left) and primitive cell of UiO-67-NBF_2 (right).[21]

The transition state (TS) calculation was performed using CP2K. The climbing image nudge elastic band (CI-NEB) method was used to locate the TS configuration. Electronic exchange and correlation were treated with the Perdew-Burke-Ernzerhof (PBE) functional. The DZVP-MOLOPT-SR basis set, the GTH pseudo potential, and the D3 correction method of Grimme were used. The cutoff energy and relative cutoff were 280 Ry and 40 Ry, respectively.

The configuration of the transition state was optimized, and the transition state configuration was confirmed through frequency analysis, which has a single imaginary frequency for a vibrational mode. The intrinsic reaction coordinate (IRC) calculation was performed in order to confirm the two minima were connected by the saddle point. The PBE functional, the augmented correlation consistent polarized valence aug-cc-pVTZ basis set, and the D3 correction method of Grimme were used. The geometries and the energies of the starting, transition state and ending configurations were obtained on the higher-level theories MP2 and CCSD(T). The aug-cc-pVQZ basis set was used. These calculations were performed using Gaussian16.

3.2 **Results and Discussions**

The gaseous hydrogenation of CO to formaldehyde reaction is shown in equation 3-2. The reaction energy (ΔE), reaction enthalpy (ΔH) and the reaction Gibbs free energy (ΔG) were first calculated with PBE, B3LYP, MP2, and CCSD(T) methods and were extrapolated to the complete basis set (CBS). As shown in Table 1, this is an entropy decreasing reaction and has positive gas phase Gibbs free energy change. The corresponding equilibrium reaction constant at 298K calculated from $K_{eq} = e^{-\Delta G/RT}$ at CCSD(T) level is 2.29×10^{-13}. We note that Bahmanpour et al.,[8] stated that the equilibrium constant is independent of temperature in the range of 298 to 628 K. This is an unusual situation and is likely due to the enthalpy of reaction being close to zero, as seen from the higher levels of theory in Table 1. Hence, we can safely say that the reaction is thermodynamically unfavorable at all reasonable temperatures.

$$CO(g) + H_2(g) \rightleftharpoons CH_2O(g) \qquad (3\text{-}2)$$

Table 1. Electronic energy, enthalpy and reaction Gibbs free energy for the formaldehyde synthesis reaction

	ΔE/eV	ΔH/eV	ΔG/eV
PBE	-0.549	-0.316	0.003
B3LYP	-0.340	-0.106	0.215
MP2	-0.245	-0.001	0.318
CCSD(T)	-0.220	0.022	0.343

To assess the kinetic feasibility of the CO hydrogenation reaction, we then calculated the uncatalyzed reaction path in the gas phase. The reaction path calculated with the PBE method was plotted and as shown in Figure 3, the rate-limiting step is the H-H bond breaking step. And

the reactants and product were connected via a C_s-symmetry transition state structure. The reaction barrier calculated from PBE, B3LYP and higher-level ab initio methods (MP2 and CCSD(T)) are very high. The barriers calculated are 2.85 eV, 3.30 eV, 3.68 eV and 3.54 eV for PBE, B3LYP, MP2, and CCSD(T), respectively, indicating the kinetic difficulty of the reaction.

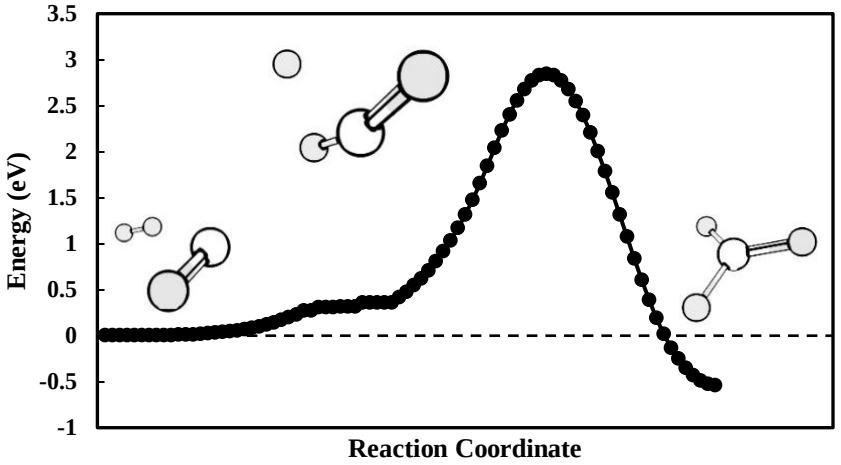

Figure 3. Energy profile of the uncatalyzed CO hydrogenation reaction.

Hence, to cope with the kinetic difficulty for the hydrogenation of CO to formaldehyde in the gas phase, the utilization of an effective catalyst is of great necessity. We calculated the reaction path for the hydrogenation reaction with the mediation of the NBF_2 moiety. The hydrogenation of carbon monoxide catalyzed by the NBF_2 moiety proceeds in three steps:

1. The physisorption of H_2 and the heterolytic dissociation of H_2 on the NBF_2 moiety.
2. The reaction between the two dissociated H* on the LP sites and carbon monoxide to form formaldehyde.
3. The desorption of produced formaldehyde to the gas phase.

For the first H_2 physisorption-dissociation step, an intermediate van der Waals complex between H_2 and the LP moiety of the UiO-67-NBF_2 was formed with an adsorption energy of -0.20 eV. Then, H_2 heterolytically dissociates on the LP moiety, one hydrogen is bound to the Lewis basic (N) site and one hydrogen is bound to the acidic (B) site. The reaction barriers are 0.46 eV and 0.76 eV for the forward and reverse reactions, respectively.[20]

The second step, as shown in Figure 4, is the rate-limiting step, which happens in a concerted Eley-Rideal-like mechanism. This reaction starts with the formation of a complex where the reactants interact with each other. Then the H^+ and H^- bound to the basic (N) and acidic sites (B) protonate the CO molecule, which results in the formation of formaldehyde. Such interpretation is confirmed by the geometry analysis, the H-N bond was elongated to 1.365 Å from an initial value of 1.033 Å, the H-B bond length was elongated to 1.424 Å from 1.236 Å, and the distances at the TS between the two H* and the C atom of the CO molecule were 1.322 Å and 1.417 Å. In addition, the IRC calculations based on the TS structure result in the expected initial and final structures, further confirming the NEB calculations.

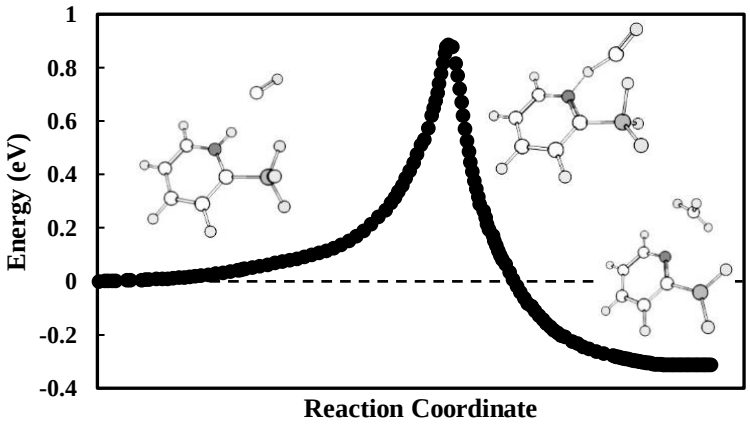

Figure 4. Energy profile of the NBF_2 moiety catalyzed CO hydrogenation reaction.

The barriers calculated are 0.92 eV, 1.37 eV, 1.53 eV and 1.67 eV for PBE, B3LYP, MP2, and CCSD(T) methods, respectively. For comparison, the hydrogenation barriers for both uncatalyzed and catalyzed reactions at PBE, B3LYP, MP2, and CCSD(T) are shown in Figure 5. Compared to the uncatalyzed gaseous reaction barrier, the hydrogenation reaction barriers catalyzed by the NBF_2 moiety were significantly reduced by ~2 eV, establishing the striking effect of the NBF_2 Lewis pairs moiety as a catalyst on the reduction of hydrogenation reaction barrier.

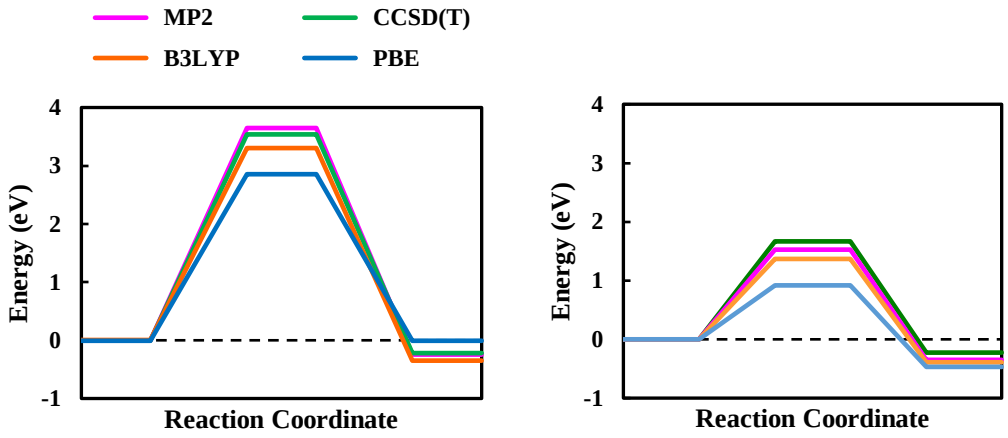

Figure 5. Comparison between uncatalyzed (left) and catalyzed (right) CO hydrogenation reaction barriers.

Compared with barriers calculated with the GGA functional (PBE), higher reaction barriers were observed with hybrid functional (B3LYP), and post-Hartree-Fock methods (MP2 and SSCD(T)), especially for MP2 and CCSD(T), the barriers are higher by about 0.7 eV. This huge difference could be resulted from the self-interaction error (SIE).[38] This result indicates that GGA functionals like PBE incorrectly predict the electron density and fail to properly describe the transition state, compared to the high-level methods.

My colleagues calculated the reaction energy diagram of the CO hydrogenation reaction inside the Lewis pair functionalized MOF, UiO-67-NBF_2, using the BEEF-vdw functional, identified the uncertainty associated with the choice of functionals and showed that the reaction is effectively irreversible in UiO-67-NBF_2. Moreover, GCMC calculations revealed that CO and H_2 have relative higher partial pressure than CH_2O, which would enhance the reaction rate and shift the reaction equilibrium toward the formation of formaldehyde. Because of the nature of LP sites, the methoxy intermediate produced in many industrial synthesis methods[6] is avoided and hence reduce the reaction steps. The production of formaldehyde was shown to be more favorable within the MOF and the produced formaldehyde can be easily separated from CO and H_2 with the excess reactants being recycled. Detailed results and discussions can be found in our published paper.[21]

3.3 **Conclusions**

Computational calculations with high-level ab initio methods were applied to study the direct formaldehyde synthesis from syngas in the gas phase. The thermodynamic data and activation barriers were reported for uncatalyzed gaseous reaction. Positive Gibbs free reaction energy and high energy barrier indicate this process highly unlikely both thermodynamically and kinetically.

Activation barriers were reduced by ~2 eV under the mediation of LP catalyst, which indicates the great importance and significant effects it plays in this reaction. Incorporating the catalytic LP moiety into UiO-67-NBF_2 retains the LP reactivity, and an estimated reaction rate (10^{-3} s^{-1} per site) at 140 °C and at near ambient pressure can be achieved.[21] Moreover, the reaction conversion will be enhanced, and the thermodynamic limitation of the gaseous reaction can be

addressed. The undesired intermediate methoxy is also avoided. In conclusion, functionalizing MOF with catalytic Lewis pairs is a promising approach for gas-phase formaldehyde synthesis from syngas.

4.0 **Olefin Paraffin Separation**

(This work will be published in a forthcoming paper, Paraffin/Olefin Separation in Metal-Organic Framework with Single Active Sites, authored by Mona H. Mohanmed, Yahui Yang, Lin Li, Sen Zhang, Götz Veser, J. Karl Johnson and Nathaniel Rosi)

4.1 **Computational Details**

The unit cell of MFU-4l was obtained from the Cambridge Crystallographic Data Center.[39] All periodic calculations were carried out on the primitive cell. The lattice constants of the optimized primitive cell are $a = b = c = 22.193$ Å, $\alpha = \beta = \gamma = 60°$.

All periodic calculations were performed in the mixed Gaussian plane wave scheme as implemented in the CP2K code, the D3 dispersion correction method of Grimme was used to approximate the van der Waals interactions. The exchange correlation energy was calculated with the PBE functional, the DZVP-MOLOPT-SR basis set, and GTH pseudo potentials. The plane wave cutoff energy and relative cutoff were 400 Ry and 60 Ry, respectively.

The periodic MOF structure was approximated with a 30-atom cluster (Figure 6). This cluster was defined in a way to best represent the local environment. The cluster configuration was optimized with the PBE functional. The triple-zeta valence polarization basis set (def2-TZVP) in combination with the D3 version of Grimme's dispersion and Becke-Johnson damping (GD3BJ) were used.

The single point energy was then calculated with the hybrid functional B3LYP with def2-TZVP basis set and GD3BJ dispersion correction. The basis set superposition error (BSSE) was corrected by the counterpoise (CP) method.

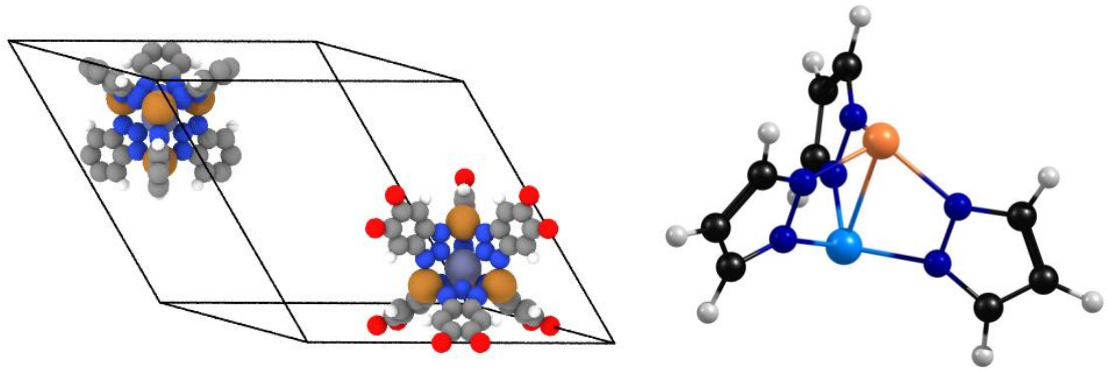

Figure 6. Primitive cell of Cu(I)-MFU-4*l* (left) and 30-atom cluster (right).

4.2 **Results and Discussions**

Compared to the calculations of binding energies in a full flexible MOF, using a 30-atom cluster will greatly reduce the computational cost. To validate the effectiveness of the tailored 30-atom cluster model compared to the full framework periodic system, binding energies on the open metal sites for a list of adsorbates were calculated for both the cluster and the full framework system using the CP2K code. For comparison, the resulting binding energies are shown in Figure 7, the solid line represents the identity line, y=x, where y means the binding energy in the periodic framework and x means the binding energy on the 30-atom cluster. Black squares represent the

adsorbates and were found to be aligned close to the solid line with a good linear correlation (the slope is 0.997 and the coefficient of determination R^2=0.98). The cluster model is hence proved to accurately describe the binding energy on the open metal sites in good agreement with the periodic system.

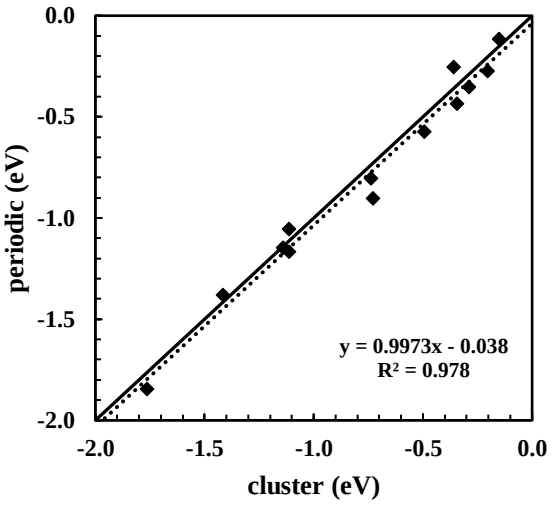

Figure 7. Comparison between the binding energies on the fully relaxed 30-atom cluster and in the periodic framework.

The cluster model was used for further investigation on improving the computation accuracy while saving computational cost. Because more DFT exchange functionals, basis sets, and correction methods can be performed in Gaussian 16 code, and calculations on small systems have been widely investigated and reliable results have been obtained using this code. Hence, the G16 code was used for cluster calculations. The consistence of binding energies calculated from CP2K and Gaussian 16 should be verified first; the binding energies on the cluster calculated from CP2K and Gaussian 16 were summarized in Table 2, CP2K code and Gaussian 16 code gave almost identical binding energies for most adsorbates. Though the percentage errors of some

binding energies are large, such as CO_2, CH_4, the absolute error is more important, and errors smaller than 0.1 eV are regarded as not significant in DFT calculations and could be due to the use of different basis sets. However, we should also notice the significant binding energy difference of CO (0.28 eV), which we don't have a reasonable explanation at this point.

Table 2. Summaries of binding energies on the fully flexible cluster calculated with CP2K and G16 code

	C_2H_4	C_2H_6	C_3H_6	C_3H_8	CO	CO_2	CH_4	N_2	H_2	H_2O	NO	NH_3
CP2K-PBE	-1.14	-0.29	-1.11	-0.35	-1.76	-0.15	-0.2	-0.74	-0.49	-0.36	-1.11	-0.73
G16-PBE	-1.14	-0.30	-1.07	-0.34	-1.48	-0.19	-0.24	-0.74	-0.43	-0.47	-1.14	-0.83

All electronic energies were further refined using the B3LYP functional with the PBE optimized geometries. And BSSE was corrected by applying the CP method. As shown in Figure 8, good agreement was observed between our calculation results and experimental results from Denysenko et al.[11] and from our collaborators, which confirms the reliability of our computational procedure.

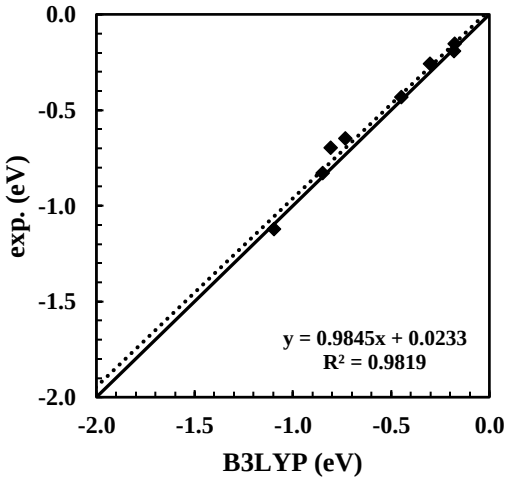

Figure 8. Comparison between the binding energies on the fully flexible 30-atom cluster and the experimental results.

It notable that the binding energies of C_2H_4, C_2H_6, C_3H_6, and C_3H_8 are -0.85 eV, -0.24 eV, -0.81 eV, and -0.29 eV, respectively, indicating that C_2H_4 (C_3H_6) binds to the open metal sites more strongly while C_2H_6 (C_3H_8) shows less affinity. Moreover, the binding energies show a big difference of 0.61 eV (0.52 eV) between C_2H_4/C_2H_6 (C_3H_6/C_3H_8), which indicates the possibility in applying the material in practical separation operations. And for separation that relies on competitive binding, a larger difference in binding energy indicates an easier and more significant separation. The DFT calculated binding geometries for C_2H_4, C_2H_6, C_3H_6, and C_3H_8 are presented in Figure 9, C_2H_4 and C_3H_6 form complexes in a side-on mode while C_2H_6 and C_3H_8 bound to the Cu(I) site via the terminal methyl group (-CH_3). The carbon-carbon double bond lengths of C_2H_4 and C_3H_6 are elongated to 1.385 Å and 1.389 Å, respectively, compared to the carbon-carbon double bond length of the free molecules (1.33 Å).

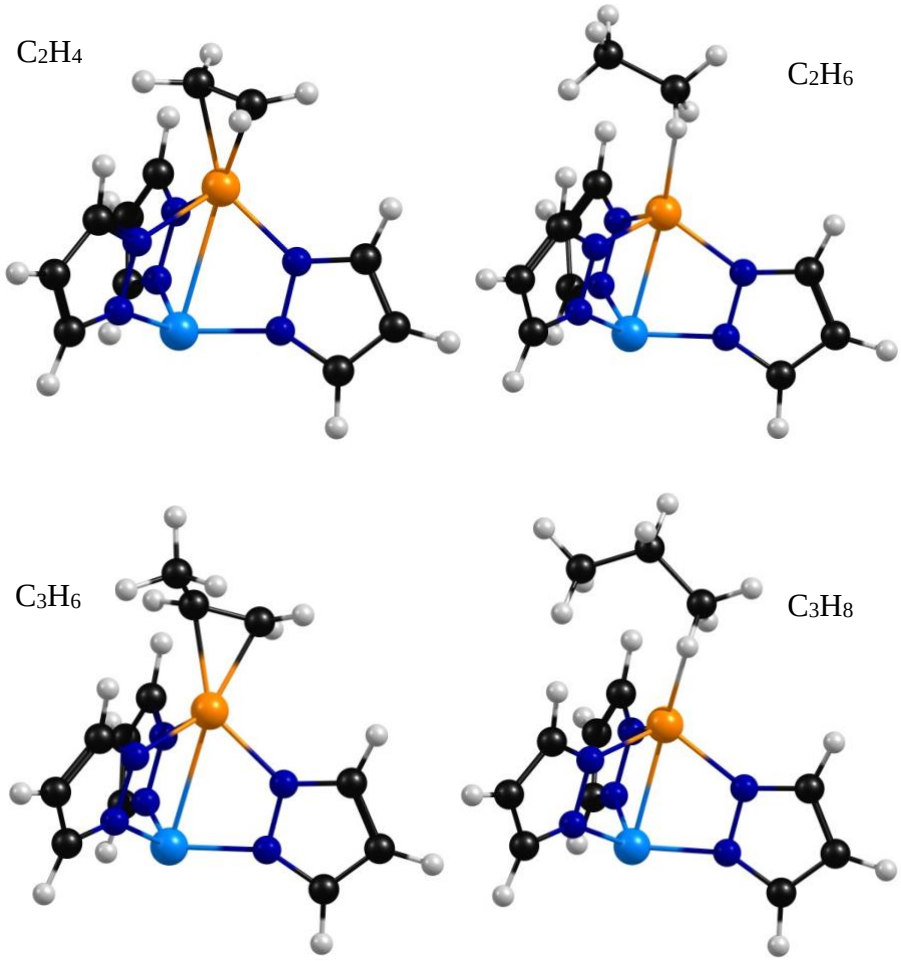

Figure 9. Binding configurations of C_2H_4, C_2H_6, C_3H_6, and C_3H_8 on the fully flexible cluster.

The difference in the binding mode and the resulting binding energy can be explained by the Dewar-Chatt-Duncanson model.[40-41] The electron configuration of Cu(I) is [Ar]3d10. It is known as π-complex-active metal for having empty outermost *s*-orbitals and is able to interact with chemicals having π-electrons like C_2H_4 and C_3H_6 in this case. For this alkene-Cu(I) system, the π-symmetry bonding orbital of the alkene carbon atoms overlap with the empty outer s-orbital of the Cu(I). And on the other hand, the Cu(I) donates electrons back from its *d* atomic orbital to the empty π^* antibonding orbitals of the alkene. These effects will reduce the carbon-carbon bond

order and hence lead to the elongated carbon-carbon distance. Additionally, our calculations also showed that 1) each Cu atom can only accept one adsorbate to bind on. 2) the un-exchanged Zn-Cl site in the original Zn-MFU-4*l* shows no chemisorption ability.

Even though the computational cost has been reduced and the desired computational results were obtained by truncating the periodic system, it is still challenging to employ higher level *ab initio* methods such as MP2. However, as shown in Figure 10, a fully rigid cluster calculation of binding energies will give large deviation compared to flexible cluster calculation and experimental results, especially for those having unsaturated bonds, indicating that the adsorbate has non-negligible impacts on the cluster structure and the binding energy.

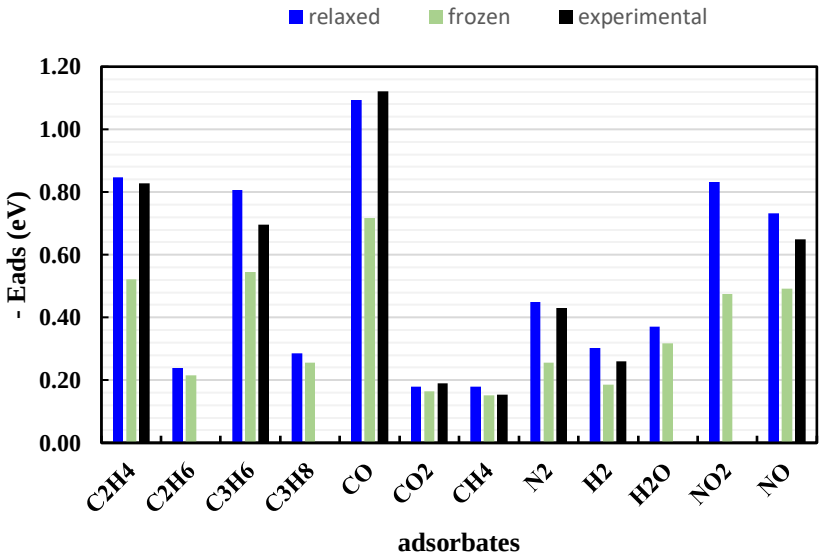

Figure 10. Comparison between the binding energies on the fully flexible cluster, on the fully rigid cluster, and experimental results.

Hydrocarbons (CH_4, C_2H_4, C_2H_6, C_3H_6, C_3H_8) were chosen to have a further look at how the geometry affects the binding energy. Due to the high symmetry of the cluster and the location of the binding site, five geometry parameters of the optimized cluster (Figure 11) were chosen for further investigation.

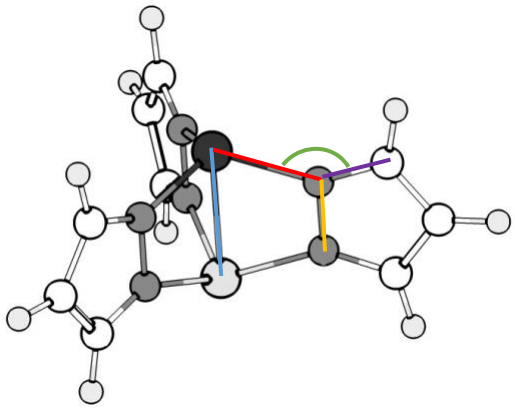

angle (Cu-N-C) **d(Cu-Zn)** **d(Cu-N)** **d(N-C)** **d(N-N)**

Figure 11. Five geometry parameters selected for the investigation on geometry-energy relationship.

The relationships between each of the five parameters and the binding energies for different adsorbates were plotted and shown in Figure 12. The binding energies on the cluster were found to be most related to three parameters, ∠(Cu-N-C), d(Cu-Zn), and d(Cu-N). These three parameters can be simultaneously changed by only relaxing the Cu atom position.

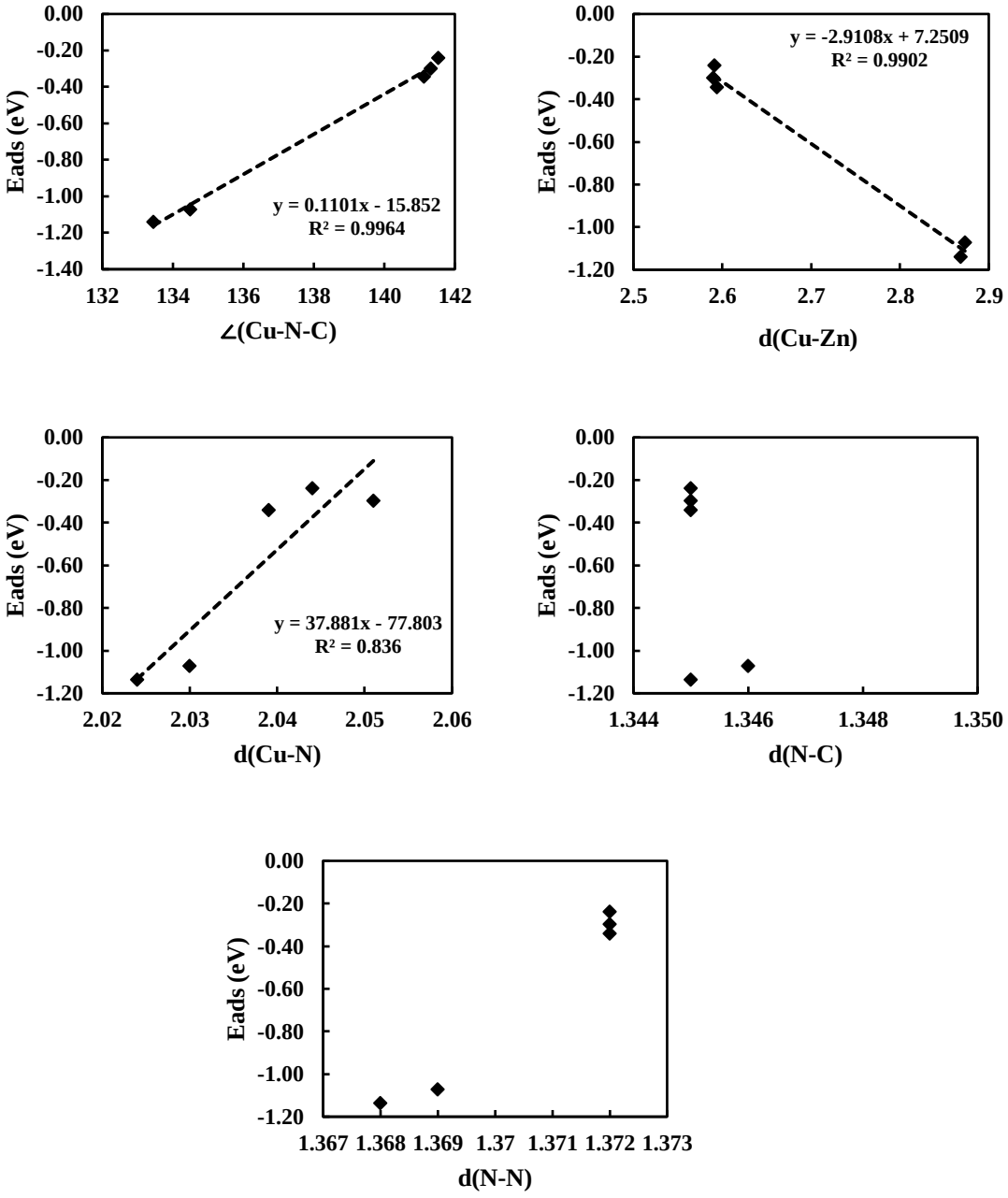

Figure 12. The correlation between ∠(Cu-N-C), d(Cu-Zn), d(Cu-N), d(N-C), d(N-N) and the binding energies for hydrocarbon adsorbates.

The binding geometries and energies were then calculated by freezing all atoms of the fully relaxed cluster except for the Cu atom. As shown in Table 3 and Figure 13, binding energies on the Cu-moveable cluster are almost identical to the all-relaxed cluster, and these values are in good agreement with experimental data.

Table 3. Summaries of binding energies on the fully flexible cluster, the fully rigid cluster, the cluster only allows Cu atom to move, and the experiment results

	flexible	rigid	allow Cu to move	exp.
CH_4	-0.18	-0.15	-	-0.15
C_2H_4	-0.85	-0.52	-0.82	-0.83
C_2H_6	-0.24	-0.21	-	-
C_3H_6	-0.81	-0.55	-0.81	-0.70
C_3H_8	-0.29	-0.26	-	-

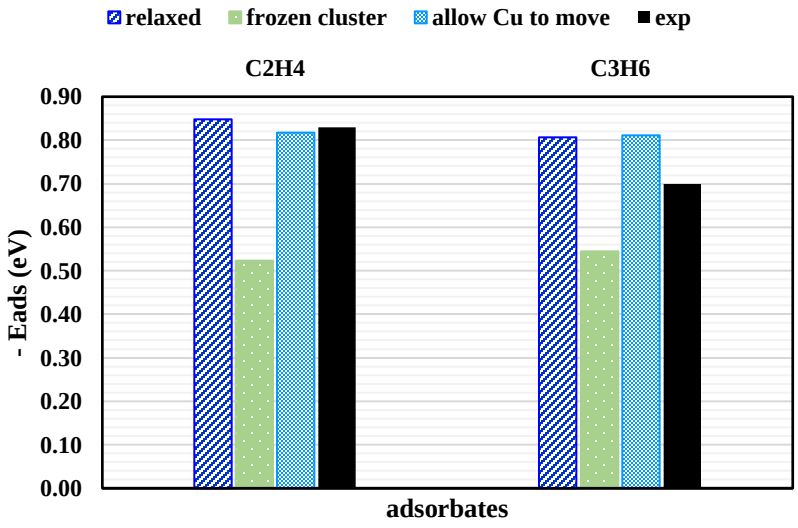

Figure 13. Comparison between the binding energies on different cluster models and experimental values.

4.3 **Conclusions**

Using Density Functional Theory (DFT), we reported accurate binding energies for a list of adsorbates on a 30-atom cluster truncated from Cu(I)-MFU-4*l*. Key parameters related to the binding energy of hydrocarbons (CH_4, C_2H_4, C_2H_6, C_3H_6, C_3H_8) are identified to enable us further to reduce the computational cost via using a rigid cluster only allowing Cu atom to move. Results from both experimental and computational results indicates olefins like C_2H_4 and C_3H_6 bind stronger than paraffins like C_2H_6 and C_3H_8 on the Cu(I) open metal sites, with a binding energy difference of 0.61 eV and 0.52 eV for C_2H_4/C_2H_6 and C_3H_6/C_3H_8, respectively. The binding modes were analyzed, and the binding energy difference is attributed to the π-complexation between the carbon-carbon double bond and the Cu(I) open metal site. Moreover, the binding energies of industrial feed steam impurities like H_2O and CO_2 on Cu(I)-MFU-4*l* are low, indicating the potential application of Cu(I)-MFU-4*l* in olefin/paraffin separation.

Appendix A Supporting Tables

Table 4. Activation barriers for catalyzed and uncatalyzed CO hydrogenation reaction via CCSD(T), MP2, DFT PBE, and DFT B3LYP calculations

Methods	Uncatalyzed (eV)	Catalyzed (eV)
PBE	2.85	0.92
B3LYP	3.30	1.37
MP2	3.65	1.53
CCSD(T)	3.54	1.67

Table 5. Summaries of binding energies on the fully flexible 30-atom cluster and in the framework for different adsorbates in CP2K code

	Cluster (eV)	Periodic (eV)
C2H4	-1.14	-1.15
C2H6	-0.29	-0.35
C3H6	-1.11	-1.06
C3H8	-0.35	-0.43
CO	-1.76	-1.85
CO2	-0.15	-0.12
CH4	-0.20	-0.28
N2	-0.74	-0.80
H2	-0.49	-0.58
H2O	-0.36	-0.25
NO2	-1.42	-1.38
NO	-1.11	-1.17
NH3	-0.73	-0.90

Table 6. Summaries of binding energies calculated from CP2K-PBE, G16-PBE, G16-B3LYP, and experimental results

	CP2K-PBE	G16-PBE	G16-B3LYP	exp
C2H4	-1.14	-1.14	-0.85	-0.83[a]
C2H6	-0.29	-0.30	-0.24	
C3H6	-1.11	-1.07	-0.81	-0.70[a]
C3H8	-0.35	-0.34	-0.29	
CO	-1.76	-1.48	-1.09	-1.12[a]
CO2	-0.15	-0.19	-0.18	-0.19[b]
CH4	-0.20	-0.24	-0.18	-0.15[b]
N2	-0.74	-0.74	-0.45	-0.43[b]
H2	-0.49	-0.43	-0.30	-0.26[b]
H2O	-0.36	-0.47	-0.37	
NO2	-1.42	-0.89	-0.83	
NO	-1.11	-1.14	-0.73	-0.65[a]
NH3	-0.73	-0.83	-0.72	

Table 7. Summaries of Zn substitution reaction energies

Substitution Reaction	Reaction Energy
$Zn_5Cl_5+CuCl_2=Zn_4CuCl_5+ZnCl_2$	-0.10154 eV
$Zn_4CuCl_5+CuCl_2=Zn_3Cu_2Cl_5+ZnCl_2$	-0.09784 eV
$Zn_3Cu_2Cl_5+CuCl_2=Zn_2Cu_3Cl_5+ZnCl_2$	-0.11849 eV
$Zn_2Cu_3Cl_5+CuCl_2=ZnCu_4Cl_5+ZnCl_2$	-0.11636 eV

Table 8. Binding energies on the flexible and the rigid cluster in G16

	flexible	rigid	ΔE
C2H4	-0.85	-0.52	0.33
C2H6	-0.24	-0.21	0.02
C3H6	-0.81	-0.55	0.26
C3H8	-0.29	-0.26	0.03
CO	-1.09	-0.72	0.38
CO2	-0.18	-0.16	0.01
CH4	-0.18	-0.15	0.03
N2	-0.45	-0.26	0.19
H2	-0.30	-0.19	0.12
H2O	-0.37	-0.32	0.05
NO2	-0.83	-0.47	0.36
NO	-0.73	-0.49	0.24

Bibliography

1.Cui, Y.; Chen, B.; Qian, G., Lanthanide metal-organic frameworks for luminescent sensing and light-emitting applications. *Coordination Chemistry Reviews* **2014,** *273-274*, 76-86.

2.Della Rocca, J.; Liu, D.; Lin, W., Nanoscale Metal–Organic Frameworks for Biomedical Imaging and Drug Delivery. *Accounts of Chemical Research* **2011,** *44* (10), 957-968.

3.Heim, L. E.; Konnerth, H.; Prechtl, M. H. G., The Prospecting Shortcut to an Old Molecule: Formaldehyde Synthesis at Low Temperature in Solution. *Chemsuschem* **2016,** *9* (20), 2905-2907.

4.Bond, G. C., *Catalysis by metals*. Academic Press: 1962.

5.Fischer, F.; Tropsch, H., Uber die Herstellung synthetischer olgemische (Synthol) durch Aufbau aus Kohlenoxyd und Wasserstoff. *Brennst. Chem* **1923,** *4*, 276-285.

6.Grabow, L.; Mavrikakis, M., Mechanism of methanol synthesis on Cu through CO2 and CO hydrogenation. *ACS Catalysis* **2011,** *1* (4), 365-384.

7.Remediakis, I. N.; Abild-Pedersen, F.; Nørskov, J. K., DFT study of formaldehyde and methanol synthesis from CO and H2 on Ni (111). *The Journal of Physical Chemistry B* **2004,** *108* (38), 14535-14540.

8.Bahmanpour, A. M.; Hoadley, A.; Tanksale, A., Critical review and exergy analysis of formaldehyde production processes. *Rev Chem Eng* **2014,** *30* (6), 583-604.

9.Bahmanpour, A. M.; Hoadley, A.; Tanksale, A., Formaldehyde production via hydrogenation of carbon monoxide in the aqueous phase. *Green Chem* **2015,** *17* (6), 3500-3507.

10.Heim, L. E.; Konnerth, H.; Prechtl, M. H. G., Future perspectives for formaldehyde: pathways for reductive synthesis and energy storage. *Green Chem* **2017,** *19* (10), 2347-2355.

11.Rybacka, O.; Czapla, M.; Skurski, P., Mechanisms of carbon monoxide hydrogenation yielding formaldehyde catalyzed by the representative strong mineral acid, H2SO4, and Lewis-Bronsted superacid, HF/AlF3. *Phys Chem Chem Phys* **2017,** *19* (27), 18047-18054.

12.Rybacka, O.; Czapla, M.; Skurski, P., The formation of formaldehyde via the carbon monoxide hydrogenation catalyzed by the HSbF6 superacid. *Theor Chem Acc* **2017,** *136* (12).

13.Stephan, D. W., Frustrated lewis pairs. *Journal of the American Chemical Society* **2015,** *137* (32), 10018-10032.

14.Stephan, D. W.; Erker, G., Frustrated Lewis pairs: metal‐free hydrogen activation and more. *Angewandte Chemie International Edition* **2010,** *49* (1), 46-76.

15.Pérez, P.; Yepes, D.; Jaque, P.; Chamorro, E.; Domingo, L. R.; Rojas, R. S.; Toro-Labbé, A., A computational and conceptual DFT study on the mechanism of hydrogen activation by novel frustrated Lewis pairs. *Phys Chem Chem Phys* **2015,** *17* (16), 10715-10725.

16.Jana, A.; Objartel, I.; Roesky, H. W.; Stalke, D., Dehydrogenation of LGeH by a Lewis N-heterocyclic carbene borane pair under the formation of L′ Ge and its reactions with B (C6F5) 3 and trimethylsilyl diazomethane: An unprecedented rearrangement of a diazocompound to an isonitrile. *Inorganic Chemistry* **2009,** *48* (16), 7645-7649.

17.Sumerin, V.; Schulz, F.; Atsumi, M.; Wang, C.; Nieger, M.; Leskelä, M.; Repo, T.; Pyykkö, P.; Rieger, B., Molecular tweezers for hydrogen: synthesis, characterization, and reactivity. *Journal of the American Chemical Society* **2008,** *130* (43), 14117-14119.

18.Yepes, D.; Jaque, P.; Fernández, I., Hydrogenation of Multiple Bonds by Geminal Aminoborane‐Based Frustrated Lewis Pairs. *Chemistry–A European Journal* **2018**.

19.Ye, J. Y.; Johnson, J. K., Design of Lewis Pair-Functionalized Metal Organic Frameworks for CO2 Hydrogenation. *ACS Catalysis* **2015,** *5* (5), 2921-2928.

20.Ye, J. Y.; Johnson, J. K., Catalytic hydrogenation of CO2 to methanol in a Lewis pair functionalized MOF. *Catal. Sci. Technol.* **2016,** *6* (24), 8392-8405.

21.Li, L.; Zhang, S.; Ruffley, J. P.; Johnson, J. K., Energy Efficient Formaldehyde Synthesis by Direct Hydrogenation of Carbon Monoxide in Functionalized Metal–Organic Frameworks. *ACS Sustainable Chemistry & Engineering* **2018**.

22.Bao, Z.; Chang, G.; Xing, H.; Krishna, R.; Ren, Q.; Chen, B., Potential of microporous metal–organic frameworks for separation of hydrocarbon mixtures. *Energy Environmental Science & Technology* **2016,** *9* (12), 3612-3641.

23.Denysenko, D.; Grzywa, M.; Jelic, J.; Reuter, K.; Volkmer, D., Scorpionate‐Type Coordination in MFU‐4l Metal–Organic Frameworks: Small‐Molecule Binding and Activation upon the Thermally Activated Formation of Open Metal Sites. *Angewandte Chemie International Edition* **2014,** *53* (23), 5832-5836.

24.Yang, R.; Kikkinides, E., New sorbents for olefin/paraffin separations by adsorption via π‐complexation. *AIChE Journal* **1995,** *41* (3), 509-517.

25.Bloch, E. D.; Queen, W. L.; Krishna, R.; Zadrozny, J. M.; Brown, C. M.; Long, J. R., Hydrocarbon separations in a metal-organic framework with open iron (II) coordination sites. *Science* **2012,** *335* (6076), 1606-1610.

26.Bao, Z.; Alnemrat, S.; Yu, L.; Vasiliev, I.; Ren, Q.; Lu, X.; Deng, S., Adsorption of ethane, ethylene, propane, and propylene on a magnesium-based metal–organic framework. *Langmuir* **2011,** *27* (22), 13554-13562.

27.Bae, Y. S.; Lee, C. Y.; Kim, K. C.; Farha, O. K.; Nickias, P.; Hupp, J. T.; Nguyen, S. T.; Snurr, R. Q., High propene/propane selectivity in isostructural metal–organic frameworks with high densities of open metal sites. *Angewandte Chemie International Edition* **2012,** *51* (8), 1857-1860.

28.Yoon, J. W.; Seo, Y. K.; Hwang, Y. K.; Chang, J. S.; Leclerc, H.; Wuttke, S.; Bazin, P.; Vimont, A.; Daturi, M.; Bloch, E., Controlled reducibility of a metal–organic framework with coordinatively unsaturated sites for preferential gas sorption. *Angewandte Chemie International Edition* **2010,** *49* (34), 5949-5952.

29.Leclerc, H.; Vimont, A.; Lavalley, J.-C.; Daturi, M.; Wiersum, A. D.; Llwellyn, P. L.; Horcajada, P.; Férey, G.; Serre, C., Infrared study of the influence of reducible iron (III) metal sites on the adsorption of CO, CO 2, propane, propene and propyne in the mesoporous metal–organic framework MIL-100. *Phys Chem Chem Phys* **2011,** *13* (24), 11748-11756.

30.Chang, G.; Huang, M.; Su, Y.; Xing, H.; Su, B.; Zhang, Z.; Yang, Q.; Yang, Y.; Ren, Q.; Bao, Z., Immobilization of Ag (i) into a metal–organic framework with–SO 3 H sites for highly selective olefin–paraffin separation at room temperature. *Chemical Communications* **2015,** *51* (14), 2859-2862.

31.Li, B.; Zhang, Y.; Krishna, R.; Yao, K.; Han, Y.; Wu, Z.; Ma, D.; Shi, Z.; Pham, T.; Space, B., Introduction of π-complexation into porous aromatic framework for highly selective adsorption of ethylene over ethane. *Journal of the American Chemical Society* **2014,** *136* (24), 8654-8660.

32.Kohn, W.; Sham, L. J., Self-Consistent Equations Including Exchange and Correlation Effects. *Physical Review* **1965,** *140* (4A), A1133-A1138.

33.Hohenberg, P.; Kohn, W., Inhomogeneous electron gas. *Physical review* **1964,** *136* (3B), B864.

34.Møller, C.; Plesset, M. S., Note on an Approximation Treatment for Many-Electron Systems. *Physical Review* **1934,** *46* (7), 618-622.

35.Schrödinger, E., Quantisierung als Eigenwertproblem. **1926,** *385* (13), 437-490.

36.Helgaker, T.; Klopper, W.; Koch, H.; Noga, J., Basis-set convergence of correlated calculations on water. **1997,** *106* (23), 9639-9646.

37.Henkelman, G.; Uberuaga, B. P.; Jónsson, H., A climbing image nudged elastic band method for finding saddle points and minimum energy paths. *The Journal of Chemical Physics* **2000,** *113* (22), 9901-9904.

38.Perdew, J. P.; Zunger, A., Self-interaction correction to density-functional approximations for many-electron systems. *Physical Review B* **1981,** *23* (10), 5048.

39.Groom, C. R.; Bruno, I. J.; Lightfoot, M. P.; Ward, S. C., The Cambridge Structural Database. *Acta Crystallographica Section B* **2016,** *72* (2), 171-179.

40.Dewar, J., A review of the pi-complex theory. *Bulletin de la Societe Chimique de France* **1951,** *18* (3-4), C71-C79.

41.Chatt, J.; Duncanson, L., 586. Olefin co-ordination compounds. Part III. Infra-red spectra and structure: attempted preparation of acetylene complexes. *Journal of the Chemical Society* **1953**, 2939-2947.